Proc. Natl. Acad. Sci. USA
Vol. 95, pp. 811–817, February 1998
Colloquium Paper

This paper was presented at a colloquium entitled "Neuroimaging of Human Brain Function," organized by Michael Posner and Marcus E. Raichle, held May 29–31, 1997, sponsored by the National Academy of Sciences at the Arnold and Mabel Beckman Center in Irvine, CA.

Functional analysis of primary visual cortex (V1) in humans

ROGER B. H. TOOTELL*, NOUCHINE K. HADJIKHANI, WIM VANDUFFEL, ARTHUR K. LIU, JANINE D. MENDOLA, MARTIN I. SERENO, AND ANDERS M. DALE

Nuclear Magnetic Resonance Center, Massachusetts General Hospital, 149 13th Street, Charlestown, MA 02129

ABSTRACT **Human area V1 offers an excellent opportunity to study, using functional MRI, a range of properties in a specific cortical visual area, whose borders are defined objectively and convergently by retinotopic criteria. The retinotopy in V1 (also known as primary visual cortex, striate cortex, or Brodmann's area 17) was defined in each subject by using both stationary and phase-encoded polar coordinate stimuli. Data from V1 and neighboring retinotopic areas were displayed on flattened cortical maps. In additional tests we revealed the paired cortical representations of the monocular "blind spot." We also activated area V1 preferentially (relative to other extrastriate areas) by presenting radial gratings alternating between 6% and 100% contrast. Finally, we showed evidence for orientation selectivity in V1 by measuring transient functional MRI increases produced at the change in response to gratings of differing orientations. By systematically varying the orientations presented, we were able to measure the bandwidth of the orientation "transients" (45°).**

Why Primary Visual Cortex?

The increasing sophistication of modern neuroimaging methods has made it possible to analyze multiple features of the functional architecture in specific cortical areas. Similar studies have been done in experimental animals by using different techniques (e.g., optical recording, deoxyglucose labeling, and single unit mapping). The human neuroimaging studies have greatly clarified the functional organization of presumptive human areas such as MT (1–7), and the retinotopy of multiple cortical visual areas (8–15). Here we combine these retinotopic and functional mapping approaches in primary visual cortex, whose borders can also be defined in the same individuals.

Area V1 is the human visual cortical area with the most well-defined anatomical boundaries, agreed on by virtually all previous studies, both historical (e.g., refs. 16–18) and more recent (e.g., refs. 19–23). In primates, area V1 plays a critical role in visual information processing, because most visual information ultimately reaching the rest of visual cortex is first funneled through V1 (24). This anatomically complicated routing task is presumably why "striate" cortex is so markedly laminated (striated); in cortex, ascending and descending inputs and outputs are anatomically segregated in different layers. In fact, primate striate cortex has been subdivided into 11 identifiable laminar divisions (1, 2, 3, 4A, 4B, 4Ca, 4Cb, 5A, 5B, 6A, and 6B) (25, 26) rather than the customary six layers described in most cortical areas.

This "gatekeeper" role of V1 in the primate cortical hierarchy may also influence the number of neurons in the area—V1 is the largest known visual cortical area, and perhaps the largest cortical area, at least in macaques, where multiple cortical area boundaries are best known (24). In human V1, ocular dominance columns have been demonstrated by using multiple anatomical stains (27–30), and in one report, functional labeling (31). Human V1 was also the focus of several early functional studies, including electrically induced phosphenes (e.g., ref. 32), retinotopic lesion defects (e.g., ref. 21), and positron-emission tomography retinotopy (33). In macaques, V1 is probably the most thoroughly studied area in visual cortex—thus furnishing very detailed predictions about what should be found in human V1.

Therefore human V1 appeared to be an ideal location to test for addition functional features within a well defined, well accepted cortical area, by using functional MRI (fMRI). We did these studies by using fMRI techniques described elsewhere (e.g., ref. 12), except that some of the data here were collected with a 3-T scanner (General Electric/Advanced NMR). This high field scanner yields activity data of somewhat higher signal/noise ratio, but otherwise similar magnetic resonance signals.

Retinotopy

As in multiple extrastriate cortical areas (5, 8–15), striate cortex can be accurately mapped *in vivo* on the basis of its fMRI retinotopy. In fact, retinotopic maps are one of the most certain criteria for defining a cortical visual area (24). Although it is well known that V1 normally extends over the depth and lips of the calcarine fissure, there is significant variability in the size, location, and shape of V1, and even more variability in the shape of the calcarine fissure (e.g., ref. 23). Thus in V1, as elsewhere in human visual cortex, the area boundaries need to be mapped *in each individual subject*—they cannot be safely generalized from other subjects or other studies, or even from the contralateral hemisphere of the same subject.

One way to map retinotopic area boundaries is to measure and calculate the field sign. Roughly, the "field sign" indicates whether the geometry of the cortical representation matches the (magnified) map polarity of the actual visual field, or whether it is inverted to that. Field sign analysis is based on paired scans revealing cortical activation to the two polar retinotopic coordinates: (*i*) eccentricity, and (*ii*) polar angle (12, 13). Fig. 1 *A* and *B* shows the location of V1 and surrounding retinotopic areas, based on field sign analysis, on left and right hemispheres of the cortical surface in its normal configuration, showing the medial bank. The location of V1 and surrounding retinotopic areas is clarified in 1C and 1D, which shows the same data in "inflated" cortical surfaces,

Abbreviations: MR, magnetic resonance; MRI, MR imaging; fMRI, functional MRI.

*To whom reprint requests should be addressed. e-mail: tootell@nmr.mgh.harvard.edu.

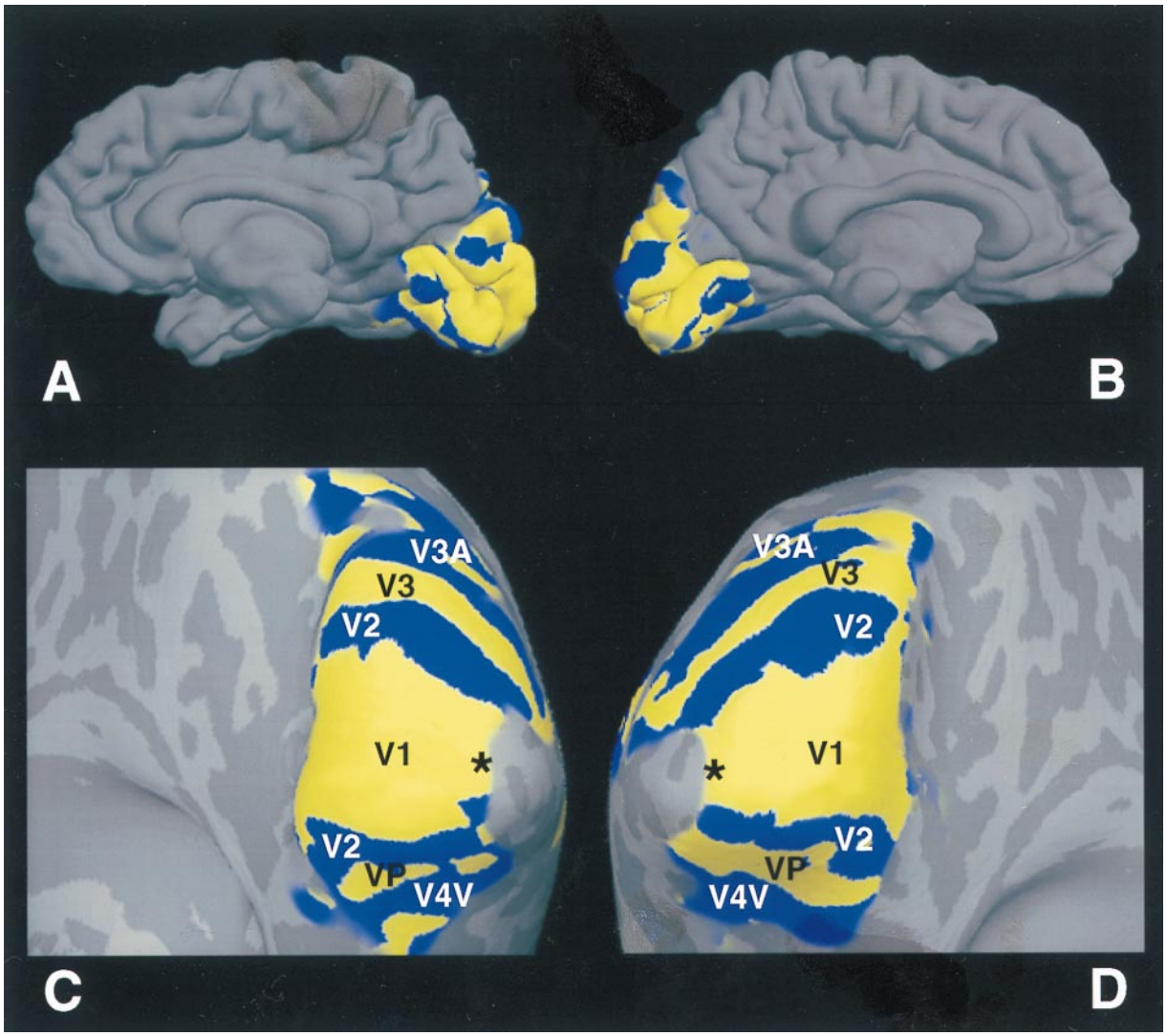

FIG. 1. Topography of primary visual cortex and surrounding areas. (*A* and *B*) Field sign analysis (12, 13) of retinotopic cortical visual areas from right and left hemispheres (respectively) in a single subject. Both hemispheres are views of the medial bank, in its normal, folded configuration. Thus in *A*, anterior is to the left, and posterior to the right. In *B*, this is reversed. The field sign maps are based on two scans measuring polar angle (rotating thin ray stimulus), and two scans measuring eccentricity (expanding thin ring stimulus), acquired from echo-planar images in a 3-T scanner (General Electric/ANMR), using a bilateral, send/receive quadrature coil. Both stimuli extended 18–25° in eccentricity (36–50° extent). (*C* and *D*) Same data, in a cortically "inflated" format, now viewed from a more posterior–inferior vantage point. Again the left panel shows the right hemisphere, and the right panel shows the left hemisphere from the same subject. Human retinotopic areas revealed by the field sign analysis have been labeled (V1, V2, V3, VP, V3A, V4v). Cortical areas with a visual field sign (polarity) similar to that in the actual visual field are coded blue, and those areas showing a mirror-reversed field polarity are coded yellow. Also labeled is the foveal representation in V1 (black asterisks). Gyri and sulci in the folded state (e.g., *A* and *B*) are coded in lighter and darker shades of gray (respectively) in the inflated format (*C* and *D*). In this subject, area V1 is somewhat larger than normal, extending well past the lips of the calcarine fissure. However, as in most subjects, the V1 representation of the extrafoveal horizontal meridian lies near the fundus of the calcarine fissure.

viewed from a posterior inferior viewpoint. In this subject, V1 extends further beyond the lips of the calcarine fissure, and onto the lateral surface, compared with most subjects.

In a previous study using the deoxyglucose labeling technique, the internal retinotopy of *macaque* V1 was revealed by stimulating with stationary, flickering, retinotopically specific check stimuli based on polar geometry (rays and rings) (34, 35). To judge more accurately the degree of similarity between humans and macaques, here we did an analogous experiment in human V1, using fMRI.

The present experiment was redesigned slightly to match two differences of the fMRI technique: (*i*) poorer spatial resolution, but (*ii*) an unlimited number of activity maps, from each fMRI subject. Here we stimulated with spatially alternating flickering check stimuli grouped into one of the following: (*i*) isopolar angle "wedges", (*ii*) isoeccentricity "rings", or (*iii*) circles of equal polar-angle diameter.

These stimuli, and the results of this stimulation, are shown in Fig. 2. Data from three scans are shown. For each scan the stimuli are shown in S1–2, S3–4, and S5–6, and the corresponding activity is shown in *A* plus *B*, *C* plus *D*, and *E* plus *F*, respectively. The activities produced by the first and second retinotopic stimuli (in each scan) are shown in red and green (respectively) in the activity maps. The activity maps are illustrated from the same hemispheres shown in Fig. 1, but now are rendered on fully flattened portions of the cortical surface.

As one might expect from a roughly polar retinotopy in macaque V1: (*i*) the isopolar-angle wedges produce roughly equal width, roughly parallel stripes in cortex; (*ii*) the isoeccentric rings of radially varying width produce stripes of roughly equal width, oriented approximately orthogonal to those in *i*; and finally (*iii*) the circles of radially varying *stimulus* diameter produced circular activity patches, of roughly equal *cortical* width. The retinotopic patterns do not extend far into

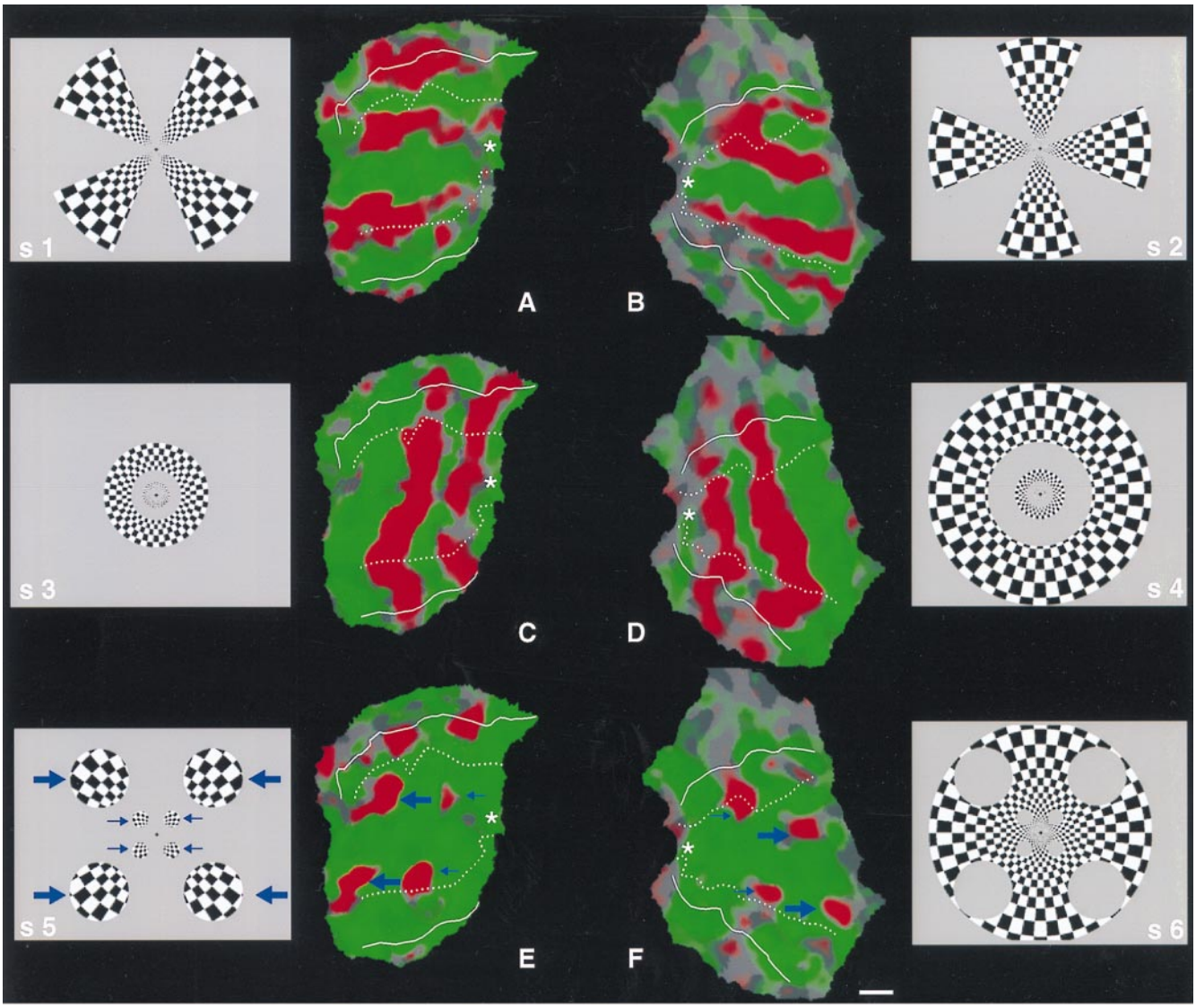

FIG. 2. Representation of stationary polar coordinate stimuli (rays and rings, respectively) in human V1. This experiment was designed to produce a "bulls-eye" or "spider web" pattern in area V1 and examine the response by using fMRI, analogous to the pattern produced in macaque V1 previously by using different functional imaging techniques (34, 35). Here, the ray and ring stimuli were presented separately, during different scan acquisitions. During the first scan, the subjects viewed alternating 16-sec epochs of ray stimuli ("S1" and "S2") composed of flickering black and white checks. This viewing produced the activity patterns shown in *A* and *B*. Preferential activation by the first stimulus is coded in red, and preferential activation by the second stimulus is coded green. *A* is a flattened section of the cortical surface from the right hemisphere, and *B* is from the left hemisphere. Both sections are taken from the same hemisphere shown in Fig. 1. Area V1 is the large middle region enclosed in dotted lines (i.e., the representation of the vertical meridian, based on the field sign map). V1 is flanked on both sides by V2, then V3/VP. The foveal representation is represented by a white asterisk. As one would expect from previous retinotopic maps in macaques and humans, rays of equal polar angle produce bands of approximately equal width in flattened cortex. During the second scan, the stimuli were composed of interleaved rings, again composed of flickering black and white checks ("S3" and "S4"). The rings were of equal polar width, thus quite unequal in width in the visual display. This stimulus produced activity bands of approximately equal width in cortex (*C* and *D*, same red–green pseudocolor conventions), oriented roughly at right angles to the bands of equal-polar-angle in *A* and *B*. During the third scan, stimuli were circular in shape (S5 and S6). The diameters of the stimulus circles were equal in polar coordinates. Thus the circles were much larger in angular subtense at greater eccentricities (large blue arrows), compared with the circles at more central eccentricities (smaller blue arrows). Nevertheless, the roughly circular activity representation of the two sets of circles in V1 was approximately equal in cortical extent (*E* and *F*). The stimulus circles are rerepresented, but progressively more faintly, in V2 and V3/VP. [The scale bar represents 1 cm (on average) across the cortical surface.]

extrastriate cortex—they are mostly in V1 and V2, with minor encroachment into V3/VP. Other fMRI evidence (12) suggests that this distribution reflects the progressive decrease in retinotopic resolution from V1 through V2, V3, VP, V3A, V4v, etc.

Mapping the Blind Spot

It is well known that the retinal array is nonuniform. Receptor photopigment, size, density, and rod/cone type all vary widely across the retina. Because of the high degree of retinotopic precision in V1, it should be possible to trace how these retinal inhomogenieties are reflected (or filled in) within V1 and subsequent retinotopic areas.

The blind spot is one of these retinal nonuniformities. In each retina, a sizable gap is formed in the receptor array due to the bundling of optic nerves from a common region exiting the eye. The blind spot is roughly 5° in diameter, centered about 15° medial to the fovea, just slightly above the horizontal meridian (see Fig. 3). During normal viewing, the blind spot is functionally "filled in" by monocular input from the opposing eye. However the blind region is not small, and its effects can

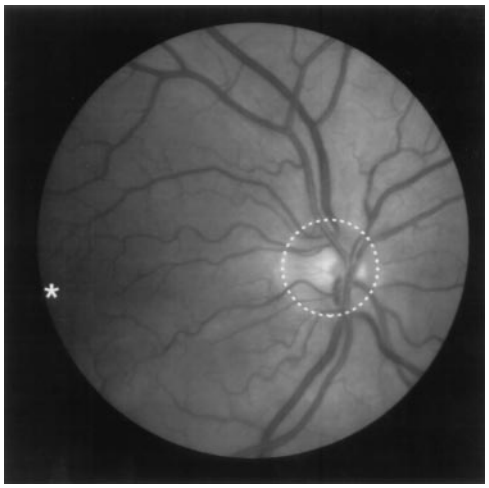

FIG. 3. Ophthalmological view of the normal retina, including the fovea (asterisk) and the optic nerve head ("blind spot," delineated by the dashed white line). In each retina, the blind spot is located nasally, and slightly superior to, the fovea. The blind spot comprises a significant region in the retina. However, its relative contribution to the cortical retinotopic map is minimized by its relatively peripheral location, convolved by the cortical magnification factor (see Fig. 4).

be demonstrated if one closes one eye and tests for vision in the appropriate visual field region. In histological tissue from V1 of macaques (35, 36) and humans (29, 30), the blind spot is represented in the input layer 4 as an elliptical, monocular region, about four ocular dominance columns wide. However, it has not been demonstrated functionally in humans by using neuroimaging techniques, to our knowledge.

The representation of the blind spot was straightforward to demonstrate in V1, by treating it as an extra-large ocular dominance column. Subjects were instructed to fixate the center of a field of scaled, black-and-white flickering checks. In this experiment, the checks extended over the entire stimulus field, throughout the experiment. When shown *binocularly*, this stimulus produced no significant differences in activity. However, when subjects viewed the stimulus *monocularly*, using either left or right eye in alternating 16-sec epochs, the representation of the monocular "blind" spot was clearly revealed (see yellow–red vs. blue–cyan spots near the middle of the left vs. right hemispheres, respectively, in Fig. 4). The monocular crescent was beyond the limits of the stimulus, so it was not activated in these experiments.

As one would predict from its location in the retina, the blind spot is located just inferior (superior in the visual field) to the cortical representation of the horizontal meridian, centered at the represented eccentricity near 15°. Although the exact size of the blind spot activation depends partly on the activity threshold, it is generally consistent with the human cortical magnification in V1 (9, 10, 13), and with the width of the blind spot representation in human histological material (29, 30). The fMRI time courses extracted from voxels in the blind spot representation (Fig. 4*A*) are quite similar to the fMRI time courses reported for conventional ocular dominance columns (31).

Contrast Sensitivity

Another major way to distinguish cortical areas is based on differences in global functional properties. Such global differences include the manipulation of visual motion to distinguish area MT from surrounding cortical areas (2, 3, 5, 11), and color to distinguish an area in the fusiform gyrus ("V4," according to refs. 2 and 3) (37, 38). Here we manipulate luminance contrast to distinguish V1 from other cortical visual areas.

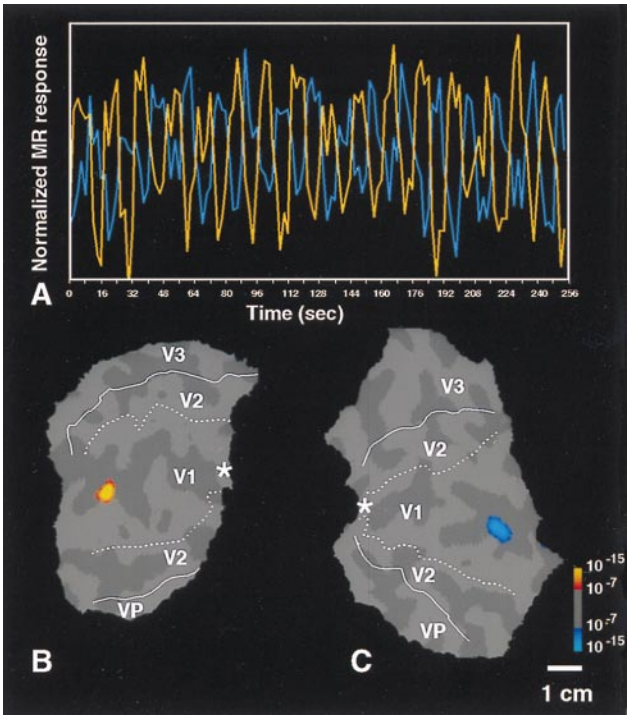

FIG. 4. Functional labeling of the representation of the retinal "blind spot," as a monocular region in V1. *B* and *C* show flattened cortical surfaces including the central two-thirds of V1, V2, and V3/VP from both left and right hemispheres (*B* and *C*, respectively) from the same subject shown in Figs. 1 and 2. During the associated experiment, the subject viewed a large stimulus composed of flickering checks, using alternating monocular stimulation in alternating 16-sec epochs. Relative to nonstimulated baseline, the stimulus produced robust activation across all of these cortical surfaces (not shown). *Preferential* activation by right vs. left eye is coded in red–orange vs. blue–cyan, respectively. The data are accumulated from one 4 min and 16 sec scan with a 3-T scanner. The high field strength is partly why the significance levels (*f* test; see statistical logo at lower right) are relatively high. The foveal representation is marked by an asterisk, and the area borders revealed by the field sign maps (Fig. 1) are transposed onto the flattened maps, as in Fig. 2. The time course of the activity in these two "blind spot" representations is shown in *A* (orange for right eye, cyan for left eye stimulation); the mutual alternation of magnetic resonance (MR) signals is quite clear. Differential activation of similar-sized stimulus "circles" in the visual field produces resolvable activation in both V1 and V2 (Fig. 2 *E* and *F*). Thus it is interesting that the representation of the blind spot does not show up in V2 (*B* and *C*), in the same subject. However, no attempt was made to equate activity thresholds across these two experiments.

In previous studies, the fMRI contrast response was measured from voxels in three cortical areas (5). In V1, the contrast response varied continuously and monotonically over contrasts greater than ≈6%. (5, 39). However, the contrast response in MT and V3 was quite different, essentially saturated at contrasts higher than ≈6% (5) (see Fig. 5*A*).

Because the contrast response functions appeared so different in striate vs. extrastriate areas, one obvious question arises: are the contrast response functions in the additional cortical visual areas relatively low in sensitivity, like those in V1? Alternatively, do they saturate quickly with high sensitivity, like those in MT and V3?

The data in Fig. 5*A* suggest that one could selectively activate V1 (relative to V3/MT, at least) by presenting two carefully chosen, alternating stimulus contrast values (6% and 95%). This presentation should produce near-maximal modulation of fMRI signals in V1, but saturated (*un*modulated) fMRI signals in high-gain extrastriate areas such as (at least) V3 and MT. In addition to confirming the earlier time course

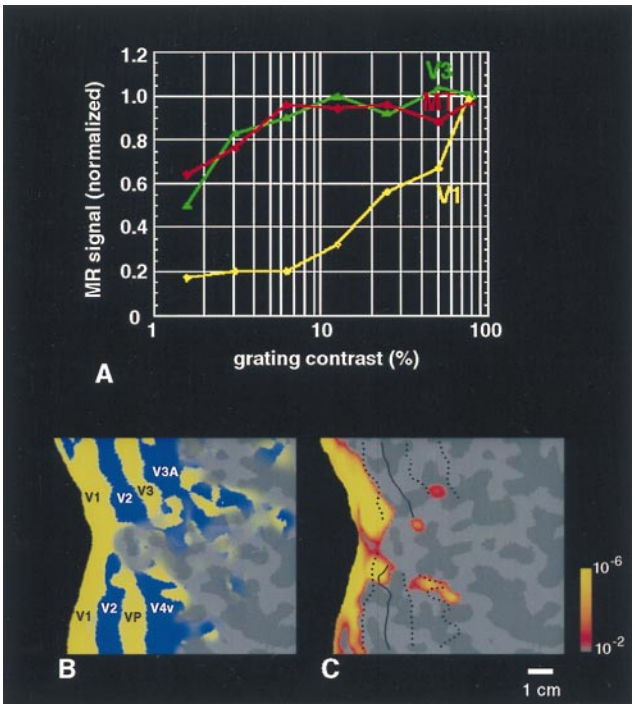

FIG. 5. Preferential activation of human V1 produced by alternating stimulus contrast. *A* shows the contrast gain function based on averaged MR time courses from three visual cortical areas: V1, V3, and MT (5). The data predict that stimulus alternation between 6% and 100% contrast should produce robust MR modulation (80% maximum) of V1, but essentially no modulation in MT and V3. *C* shows the result of this experiment. Significant activation (red through yellow) is largely confined to area V1. Area borders in *C* have been transposed from field sign tests from the same subject, shown in *B*. To minimize cortical distortion, area V1 has been artificially bisected (as in refs. 5 and 12).

information from V1 and MT in an activity map format, this experiment was thus designed to give an overall view of the contrast response functions of the many additional extrastriate areas.

Moving square wave gratings (0.7 cycle/°, 6°/sec) of 6% and 95% contrast were presented in 16-sec epochs, alternating throughout the scan (duration: 4 min, 16 sec). To minimize optokinetic nystagmus, the gratings were presented in a radial rather than a one-dimensional configuration, and the direction of motion was reversed every 2 sec to prevent motion aftereffect (6).

The 6–95% contrast modulation activated a large region in and surrounding the calcarine fissure (Fig. 5*C*). For comparison, retinotopic area boundaries (Fig. 5*B*) defined previously in this same subject by the field sign calculations (see Fig. 1) have been transposed onto the same hemisphere. The area activated by the *retinotopically invariant* contrast modulation (Fig. 5*C*) was confined approximately to V1, as defined by entirely different, *retinotopic* criteria. In control scans, we presented gratings spanning a lower contrast range (0 vs. 6%). This stimulus alternation did *not* activate V1, but it did activate MT and V3/V3A (not shown), as predicted from Fig. 5*A*. This finding strongly suggests that V1 has lower contrast sensitivity than many or all extrastriate cortical areas. It also suggests that contrast sensitivity increases by probability summation in the progressively larger receptive fields of extrastriate cortex, as suggested by some models (40).

Orientation Sensitivity

The typical fMRI experiment tests for a difference in response amplitude during several tens of seconds of stimulation with one stimulus, compared with a subsequent epoch of equal length, using a control stimulus. Unfortunately, some stimulus dimensions do not lend themselves to this approach. For instance, how would one test for the presence or absence of orientation selectivity in a given area? In animal experiments, electrophysiological studies suggest that approximately equal numbers of neurons will respond at essentially equal levels to stimuli of differing orientations (e.g., refs. 41–43). If the same is true in humans, sustained stimulation with gratings of *one* orientation should produce levels of activation that are equal to (i.e., no different from) that produced by control stimulation with gratings of a *different* orientation. Thus, tests to identify such dimensions in human visual cortex require a different approach.

One way to do this is to use high-resolution fMRI to directly visualize cortical columns that respond selectively to different orientations or directions (e.g., ref. 31). However, there is no guarantee that all interesting functional distinctions are anatomically segregated into systematic cortical columns, and it is not technically trivial to do high-resolution fMRI.

Here we describe an alternative approach, applied to demonstrating and measuring orientation sensitivity in human V1. It exploits the fact that prolonged neural responses to a given orientation will adapt slightly over time, so that useful information can be gained by looking at the postadaptation fMRI response. This approach was distilled from an earlier study in which differential fMRI responses were obtained after adaptation to different stimulus *directions* in human area MT (6).

In the present experiments, subjects fixated the center of a black/white grating during fMRI scanning. Every 0.4 sec, each stripe within the grating was varied randomly in width (range = 0.1–2°) and in position ("phase," if it had been a square-wave grating). These frequent changes in the grating configuration were designed to prevent retinal aftereffects or cortical habituation.

In the first experiment (Fig. 6 *A* and *B*), grating orientation changed 90° every 40 sec, from one oblique orientation to the other. Both grating orientations were thus 45° to vertical/horizontal, but maximally different from each other in terms of orientation.

Fig. 6*A* shows the averaged time course from V1. Fig. 6*B* shows the averaged "change-of-orientation transient," from the data in Fig. 6*A*. About 7 sec after the actual change in stimulus orientation, the averaged MR signal shows a transient increase. The 7-sec delay is consistent with the known hemodynamic delay in fMRI experiments. The 90° changes in grating orientation produce a transient positive response in fMRI signals.

In subsequent experiments we demonstrated that *smaller* angular changes in orientation produce correspondingly smaller fMRI "transients." By systematically varying the orientation (Fig. 6*C*), we were able to measure the bandwidth of this fMRI orientation selectivity (≈45°, half-width at half-height; Fig. 6*D*) in V1. This bandwidth is essentially equal to that found in a previous study measuring the human orientation bandwidth by using visual evoked potentials (44), but it is arguably wider than that predicted by single unit reports in cats and monkeys.

In preliminary tests using the flattened cortical format and stimuli that were specific for both retinotopy and orientation, we also found that such signals appear to be retinotopically specific, and preferentially located in areas V1 and V2, and to a lesser extent V3 and VP (not shown). This is similar to the topography of orientation selectivity in macaque visual cortex, as measured by single units (e.g., ref. 45).

Conclusions

This study benefited greatly from the wealth of previous data in area V1 of humans and other mammalian species. In

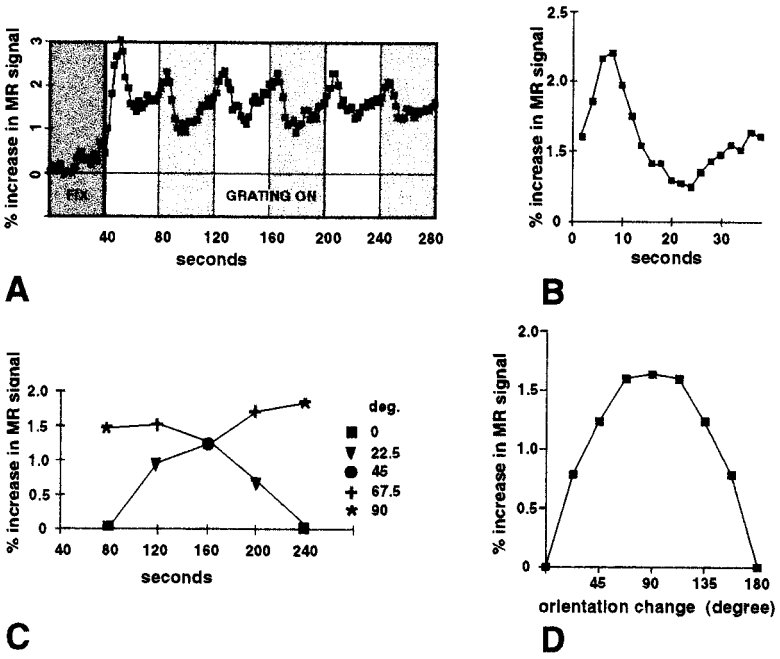

FIG. 6. Transient MR signal changes reveal orientation selectivity in human V1. Subjects fixated the center of the stimulus screen during MR scans, in a 1.5-T scanner. In *A*, scans were 4 min and 40 sec long. During the first 40 sec, the stimulus was a uniform gray field (dark gray time bin in *A*). During the remaining 4 min, the grating was presented continuously, with stripe width (0.1–2°) and position varied randomly every 0.4 sec. The flickering gratings were presented at a single orientation for 40 sec at a time. Every 40 sec, the grating orientation changed from one oblique orientation to the other, each 90° different from each other (white and light gray time bins in *A*). Signals were acquired continuously (1 image per slice per 2 sec) from voxels in area V1, selected on the basis of field sign map boundaries. *A* shows the averaged time course from 20 scans in one subject, in one ≈2-hr scan session. *B* shows the averaged response to each *change* in orientation; thus it represents the average of all epochs of a single orientation except the first grating presentation in each scan. Approximately 7 sec (the expected hemodynamic delay) following each change in orientation, a positive inflection (the "orientation transient") is produced in the averaged MR signal (*A* and *B*). The second set of experiments (*C* and *D*) shows that *smaller* angular changes in orientation produce correspondingly smaller fMRI "transients." *C* shows the average increase in signal between the actual time of orientation change (time = 0 sec) and the MR signal 6–8 sec later, when the transient MR response occurred. These changes were measured during two sets of scans, corresponding to the two curves shown in *C*. In one set of scans, the change in orientation between epochs began at 90°, becoming progressively smaller (67.5°, 45°, 22.5°, then 0°) at each subsequent epoch. During the second set of scans (presented in interleaved fashion with the first set of scans), the order of the size of orientation change was reversed (0°, 22.5°, 45°, 67.5°, then 90°). The values obtained after a specific size of orientation change were similar irrespective of presentation order, and they were averaged together to produce the average bandwidth shown in *D*. Averaged values for each orientation change in *C* are displayed twice in *D* (excepting the 90° change), for illustrative purposes.

addition to telling us where V1 is usually located, prior studies from V1 in macaques and humans had already suggested a high degree of retinotopic precision and a polar organization of the V1 retinotopy ((e.g., refs. 9, 10, 13, 34, 35, 46, 47), monocular dominance in the blind spot representation (29, 30, 35, 36), orientation selectivity (e.g., refs. 41–43), and even the averaged contrast gain functions (5, 48). In this sense the present study has value as a "calibration" or "confirmation" study.

However, some other aspects of the present study are more novel. The tests for orientation selectivity based on transient fMRI signals are an approach that could easily be generalized to tests for similarly coded stimulus dimensions, such as visual motion, color, etc. The tests for the blind spot representation could likewise be generalized to trace where and when other retinal inhomogenieties (e.g., rod/cone ratio changes with eccentricity, etc.) are "filled in" in cortex. For instance, it is interesting that the monocular blind spot representation does not appear in V2 (Fig. 4), although a binocular stimulus of almost equal dimensions is represented in V2 (Fig. 2). Because we are largely unconscious of these retinal variations, this issue also bears on the question of which cortical visual areas, and what functional aspects of visual processing, have access to conscious perception (e.g., ref. 49). Finally, the maps of contrast sensitivity (Fig. 5) suggest that contrast gain may be better accounted for by considering models of probability summation within progressively larger receptive fields (e.g., ref. 40), rather than in terms of predominant input from either magnocellular or parvocellular "streams" (e.g., refs. 5 and 48).

We thank Mary Foley, Terrance Campbell, William Kennedy, Bruce Rosen, and Thomas Brady for invaluable assistance during the course of this project. We are especially grateful to Dr. Stephan Brandt for helping to acquire some of the data. This work was supported by grants from the Human Frontiers Science Program and the National Eye Institute to R.B.H.T., the Swiss Fonds National de la Recherche Scientifique to N.K.H., and the McDonnell–Pew Foundation to J.D.M.

1. Lueck, C. J., Zeki, S., Friston, K. J., Dieber, M.-P., Cope, P., Cunningham, V. J., Lammertsma, A. A., Kennard C. & Frackowiak, R. S. J. (1989) *Nature (London)* **340,** 386–389.
2. Zeki, S., Watson, J. D. G., Lueck, C. J., Friston, K. J., Kennard, C. & Frackowiak, R. S. J. (1991) *J. Neurosci.* **11,** 641–649.
3. Watson, J. D. G., Myers, R., Frackowiak, R. S. J., Hajnal, J. V., Woods, R. P., Mazziota, J. C., Shipp, S. & Zeki, S. (1993) *Cereb. Cortex* **3,** 79–94.
4. Dupont, P., Orban, G. A., DeBruyn, B., Verbruggen, A. & Mortelmans, L. (1994) *J. Neurophysiol.* **72,** 1420–1424.
5. Tootell, R. B. H., Reppas, J. B., Kwong, K. K., Malach, R., Born, R. T., Brady, T. J., Rosen, B. R. & Belliveau, J. W. (1995) *J. Neurosci.* **15,** 3215–3230.
6. Tootell, R. B. H., Reppas, J. B., Dale, A. M., Look, R. B., Malach, R., Jiang, H.-J., Brady, T. J. & Rosen, B. R. (1995) *Nature (London)* **375,** 139–141.
7. McCarthy, G., Spicer, M., Adrignolo, A., Luby, M., Gore, J. & Allison, T. (1995) *Hum. Brain Mapp.* **2,** 234–243.
8. Schneider, W., Noll, D. C. & Cohen, J. D. (1993) *Nature (London)* **365,** 150–153.
9. Engel, S. A., Rumelhart, D. E., Wandell, B. A., Lee, A. T., Glover, G. H. E., Chichilnisky, J. & Shadlen, M. N. (1994) *Nature (London)* **370,** 106.

10. Engel, S. A., Glover, G. H. & Wandell, B. A. (1997) *Cereb. Cortex* **7,** 181–192.
11. Tootell, R. B. H., Dale, A. M., Sereno, M. I. & Malach, R. (1966) *Trends Neurosci.* **19,** 481–489.
12. Tootell, R. B. H., Mendola, J. D., Hadjikhani, N. K., Ledden, P. J., Liu, A. K., Reppas, J. B., Sereno, M. I. & Dale, A. M. (1997) *J. Neurosci.* **17,** 7060–7078.
13. Sereno, M. I., Dale, A. M., Reppas, J. B., Kwong, K. K., Belliveau, J. W., Brady, T. J., Rosen, B. R. & Tootell, R. B. H. (1995) *Science* **268,** 889–893.
14. DeYoe, E. A., Carman, G. J., Bandettini, P., Glickman, S., Wieser, J., Cox, R., Miller, D. & Neitz, J. (1996) *Proc. Natl. Acad. Sci. USA* **93,** 2382–2386.
15. DeYoe, E. A, Bandettini, P., Neitz, J., Miller, D. & Winans, P. (1994) *J. Neurosci. Methods* **54,** 171–187.
16. Gennari, F. (1782) *Francisci Gennari Parmensis Medicinae Doctoris Collegiati de Peculiari Structura Cerebri Nonnullisque Eius Morbis—Paucae Aliae Anatom. Observat. Accedunt.* (Regio Typographeo, Parma, Italy).
17. Vic-D'Azyr, F. (1786–89) *Traité d'Anatomie et de Physiologie; Vol 1, Anatomie et Physiologie du Cerveau; Vol 2, Planches Anatomiques* (Didot, Paris).
18. Baillarger, J.-P. (1840) *Mem. Acad. Med. Paris* **8,** 148.
19. Brodmann, K. (1909) *Vergleichende Lokalisationslehre der Grosshirnrinde in ihren Prinzipien dargestellt auf Grund des Zellenbaues* (Barth, Leipzig, Germany). Second printing 1925.
20. Von Economo, C. & Koskinas, G. N. (1925) *Die Cytoarchitektonik der Hirnrinde des erwachsenen Menschen* (Springer, Vienna).
21. Holmes, G. & Lister, W. T. (1916) *Brain* **39,** 34.
22. Polyak, S. (1933) *J. Comp. Neurol.* **57,** 541.
23. Stensaas, S. S., Eddington, D. K. & Dobelle, W. H. (1974) *J. Neurosurg.* **40,** 747–751.
24. Felleman, D. J. & Van Essen, D. C. (1991) *Cereb. Cortex* **1,** 1–47.
25. Lund, J. S. (1988) *Annu. Rev. Neurosci.* **11,** 253–288.
26. Hendry, S. H., Huntsman, M. M. Vinuela, A., Mohler, H., de Blas, A. L. & Jones, E. G. (1994) *J. Neurosci.* **14,** 2383–2401.
27. Haseltine, E. C., DeBruyn, E. J. & Casagrande, V. A. (1979) *Brain Res.* **176,** 153–158.
28. Hitchcock, P. F. & Hickey, T. L. (1980) *Brain Res.* **182,** 176–179.
29. Horton, J. C. & Hedley-Whyte, E. T. (1984) *Phil. Trans. R. Soc. London B* **304,** 255–272.
30. Horton, J. C., Dagi, L. R., McCrane, E. P. & DeMonasterio, F. M. (1990) *Arch. Ophthalmol.* **108,** 1025–1031.
31. Menon, R., Ogawa, S., Strupp, J. P. & Ugurbil, K. (1997) *J. Neurophysiol.* **77,** 2780–2787.
32. Penfield, W., Jaspers, H. & McNaughton, F. (1954) *Epilepsy and the Functional Anatomy of the Human Brain* (Little, Brown, Boston).
33. Fox, P. T., Miezin, F. M., Allman, J. M., Van Essen, D. C. & Raichle, M. E. (1987) *J. Neurosci.* **7,** 913–922.
34. Tootell, R. B. H., Silverman, M., Switkes, E., DeValois, R. L. (1982) *Science* **218,** 902–904.
35. Tootell, R. B. H., Silverman, M. S., Hamilton, S. L., Switkes, E. (1988) *J. Neurosci.* **8,** 1531–1568.
36. Horton, J. C. (1984) *Phil. Trans. R. Soc. Lond. B* **304,** 199–253.
37. Sakai, K., Watanabe, E., Onodera, Y., Uchida, I., Kato, H., Yamamoto, E., Koizumi, H. & Miyashita, Y. (1995) *Proc. R. Soc. London B* **261,** 89–98.
38. Kleinschmidt, A., Lee, B. B., Requardt, M. & Frahm, J. (1996) *Exp. Brain Res.* **110,** 279–288.
39. Boynton, G. M., Engel, S. A., Glover, G. H., Heeger, D. J. (1996) *J. Neurosci.* **16,** 4207–4221.
40. Watson, A. B. (1992) *Vis. Neurosci.* **8,** 65–76.
41. Hubel, D. H. & Wiesel, T. N. (1974) *J. Comp. Neurol.* **158,** 267–294.
42. Bonhoffer, T. & Grinvald, A. (1993) *J. Neurosci.* **13,** 4157–4180.
43. Hubel, D. H. & Wiesel, T. N. (1962) *J. Physiol. (London)* **160,** 106–154.
44. Jakobsson, P. (1985) *Acta Ophthalmol. (Copenhagen)* **63,** 183–191.
45. Zeki, S. (1978) *J. Physiol. (London)* **277,** 273–290.
46. Daniel, P. M. & Whitteridge, D. (1961) *J. Physiol (London)* **159,** 203–221.
47. Hubel, D. H. & Wiesel, T. N. (1974) *J. Comp. Neurol.* **158,** 295–306.
48. Sclar, G., Maunsell, J. H. R. & Lennie, P. (1990) *Vision Res.* **30,** 1–10.
49. Crick, F. & Koch, C. (1995) *Nature (London)* **375,** 121–123.